**Climate
of the Past
Discussions**

Arctic sea ice in the mid-Holocene Paleoclimate Modelling Intercomparison Project 2 simulations

M. Berger[1,2]**, J. Brandefelt**[1,2]**, and J. Nilsson**[2,3]

[1]Linné Flow Centre, Dept. of Mechanics, Royal Institute of Technology, Stockholm, Sweden
[2]Bert Bolin Centre for Climate Research, Stockholm University, Stockholm, Sweden
[3]Dept. of Meteorology, Stockholm University, Stockholm, Sweden

Correspondence to: M. Berger (marit@mech.kth.se)

CPD

8, 3445–3480, 2012

**Arctic sea ice in
PMIP2 simulations**

M. Berger et al.

Title Page

Abstract	Introduction
Conclusions	References
Tables	Figures

◀◀	▶▶
◀	▶
Back	Close

Full Screen / Esc

Printer-friendly Version

Interactive Discussion

Full Screen / Esc

Printer-friendly Version

Interactive Discussion

Discussion Paper | Discussion Paper | Discussion Paper | Discussion Paper

Abstract

The Arctic sea ice in the mid-Holocene simulations of 11 coupled global circulation models part of the Paleoclimate Modelling Intercomparison Project phase 2 (PMIP2) is analysed in this study. The work includes a comparison of the mid-Holocene sim-
ulations to the pre-industrial control simulations for each individual model and also a model-model comparison. The forcing conditions in the mid-Holocene and pre-industrial simulations differ in the atmospheric methane concentration and the latitudinal and monthly distribution of solar insolation (due to differences in the orbital parameters). Other studies have found that the difference in insolation, with increased
northern hemisphere summer insolation, explain the major differences between the simulated mid-Holocene and pre-industrial climates. The response of the simulated sea ice extent and thickness to the changes in solar insolation and atmospheric greenhouse gases is investigated. The model-model variation in pre-industrial simulated Arctic sea ice is large, with sea ice area extent ranging from 10.1 to 28.2 (7.01 to 24.6) million km^2
in March (September), and the maximum sea ice thickness ranging from 1.5 m to more than 5 m in both September and March. Nevertheless, all models agree on the sign of the difference between mid-Holocene and pre-industrial in both March and September. All models have smaller summer sea ice extent and thinner ice cover in all seasons in the mid-Holocene climate compared to the control (pre-industrial) climate. The reduc-
tion in sea ice extent is mostly confined to the sea ice margins, whereas the thinning of the ice occurs over the entire ice cover. In addition, the models also experience an enhanced summer warming north of 60° N. For the central Arctic region, models with thicker ice in the mean state in the control simulation experience the largest change in the mean state between the two climates. Comparison to available Climate Model
Intercomparison Project 3 (CMIP3) simulations with the same model version and atmospheric CO_2 concentration increased to a doubling has also been performed. The sea ice response in this future scenario is stronger than the response in the mid-Holocene simulation. Again we find that the model with the thickest mean state has the largest response.

Full Screen / Esc

Printer-friendly Version

Interactive Discussion

1 Introduction

The rapid decline in the recently observed Arctic sea ice extent as well as in future climate projections motivates more detailed studies of past evolution and variability in this region. In this study the Arctic sea ice extent and thickness in the most recent geological warm period, the early to mid-Holocene, as simulated by the models participating in the Paleoclimate Modelling Intercomparison Project Phase 2 (PMIP2), is analysed.

In recent years considerable attention has been drawn to the declining Arctic sea ice cover. In the late 1970s the first satellites were launched, enabling monitoring of the Arctic region and the sea ice cover. The median sea ice extent during the period 1979–2000 has ranged from a maximum of 16 million km^2 in March to a September minimum of 7 million km^2 (Serreze et al., 2007). However, overall the Arctic sea ice extent has declined since 1979. In September 2007 the ice covered an area of 4.3 million km^2 which is the smallest coverage observed since the satellite observations began in 1979 (Stroeve et al., 2007). The changes observed in the sea ice extent since the late 1970-ties are mainly confined to the coasts of Alaska and Siberia, with smaller changes along the northern coast of Greenland and the Canadian Archipelago (Cavalieri et al., 2008). The reduction in sea ice cover observed the recent year are most likely due to anthropogenic climate change (Notz and Marotzke, 2012).

It is not only a reduction in the sea ice cover that has been observed recently, also a reduction in thickness has been detected. The thinning is observed over the entire Arctic Ocean (Kwok and Rothrock, 2009; Rothrock et al., 2003), and is mainly a result of a reduction of the thick multi-year ice. During the same period the increase in surface temperature in the Arctic region exceeded 2 °C, which is twice as much as the global average temperature increase (Solomon et al., 2007).

Sea ice is present in the high latitudes of both hemispheres and plays an important role in the climate system. The sea ice has high albedo, and reflects most of the incoming solar radiation in the northern high latitudes. If the ice cover is replaced by open water with low albedo, more insolation will be absorbed which in turn will act as

M. Berger et al.

Printer-friendly Version

Interactive Discussion

a positive feedback, leading to enhanced warming. The ice albedo effect is believed to act to increase the Arctic Amplification. The disappearance of the Arctic sea ice could have consequences beyond the Arctic region, one example is that more open water in the Arctic can have an effect on the weather in the mid-latitudes (Petoukhov and

5 Semenov, 2010). The present and future state of the Arctic sea ice are therefore highly interesting subjects.

No model is able to predict the drastic decline observed the last decades (Stroeve et al., 2007). With respect to global warming and Arctic Amplification, what could happen in the future is of high relevance. Several different emission scenarios have been con-

10 structed to capture a wide range of possible future outcomes. Some of the models in IPCC AR4 predicts an ice free Arctic as early as 2050, the majority of the models are ice free by the end of the twenty first century (e.g. Holland et al., 2008; Stroeve et al., 2007; Zhang and Walsh, 2006).

To get a better understanding of how the Arctic sea ice may respond to future an-

15 thropogenic altering of the atmospheric greenhouse gas concentrations, a better understanding of the past evolution of the Arctic sea ice in response to variations in the forcing and boundary conditions is important. The Paleoclimate Modelling Intercomparison Project phase 2 (PMIP2) make use of state-of-the art climate models to simulate climates radically different from present day conditions. The focus of the project

20 is both model-model comparison and model-data comparison (Braconnot et al., 2007). Two of the periods frequently used for comparisons are the mid-Holocene (MH) warm period, approximately 6000 yr before present (6 ka BP), and the last glacial maximum (LGM), approximately 21 ka BP. For more information about PMIP2 see the web page, http://pmip2.lsce.ipsl.fr/. The models used in this work are part of the second phase of

25 PMIP, and the models are coupled atmosphere-ocean models.

Satellite observations of the Arctic sea ice cover exist from 1979 and onwards. Further back in time historical records and proxy data can be used to reconstruct past sea ice covers. Land erosion, fossils, and driftwood are all examples of sea ice proxies (e.g. de Vernal et al., 2008; Polyak et al., 2010). The fact that sea ice is highly variable, and

the limited temporal resolution of the data reconstruction makes the comparison to the proxy data difficult (Zhang et al., 2010). Sea ice has been present in the Arctic region the last 46 Ma (million years), but during this time the spatial extent of the ice cover has varied (Polyak et al., 2010). Several independent proxies indicate that there was a minimum in the sea ice cover between 8.5 and 6 ka BP, and during this period the region northeast of Greenland may have been seasonally ice free (Funder et al., 2011; Jakobsson et al., 2010; Polyak et al., 2010). This result is derived from proxies including driftwood, bowhead whale fossils and coastal erosion. Other proxies, based mainly on sea floor sediments indicate that the sea ice cover was more extensive northeast of Greenland at the same time (de Vernal et al., 2008).

The focus of this work has been to study the Arctic sea ice in the MH simulations in PMIP2. Both the response in sea ice area, sea ice thickness and surface temperature due to the MH forcing have been investigated, and compared to the PI simulations. From here on, by response we mean the difference due to the forcing between the MH and pre-industrial (PI) control simulations. The models are found to have a similar response to the changes in the forcing in September, with higher temperatures and smaller and thinner sea ice in the MH climate. The largest difference in the September sea ice cover between MH and PI is found in the sea ice thickness, with smaller changes in the sea ice area.

The models and experiments investigated in this paper are described in more detail in Sect. 2. A simple model describing the melt and growth of the sea ice, first introduced in Thorndike (1992) and then later in Bitz and Roe (2003) is described in Sect. 3. This model is used to analyse the difference in sea ice thickness as a function of the difference in forcing condition between MH and PI simulations. The spatial patterns of sea ice concentration, thickness and temperature in both the PI simulation and the MH simulation are analysed in Sect. 4. Here we also consider the response in the seasonal variation of the sea ice thickness in the warmer MH climate.

2 Models and experiments

2.1 Experimental design

The experimental set up for the simulations follows the PMIP2 protocol (Braconnot et al., 2007). The PI experiment is set up with a pre-industrial climate (1750 AD climate), with orbital parameters of 1950 AD and trace gases corresponding to 1750 AD. The difference in solar insolation due to the change in orbital parameters from 1750 AD to 1950 AD is negligible (Braconnot et al., 2007). The initial ocean state used for the PI experiment is modern, and the initial salinity and ocean temperature should be taken from the Levitus et al. dataset from 1998. For the MH simulations the initial salinity and ocean temperature should either be year 100 of the control run or taken from Levitus et al. (1998).

The different forcing parameters in the MH and PI climates are listed in Table 1. The orbital configuration in the MH climate result in an increase in summer and annual mean insolation in the Northern Hemisphere compared to the control simulation. Both the PI simulations and the MH simulations have been run with present day vegetation and modern ice sheets, coastlines and topography. The reference for present day vegetation is model dependent, each group uses their own vegetation. The solar constant used for all experiments is 1365 W m^{-2}.

The difference between the PI and MH solar insolation is more important in terms of radiative forcing than the trace gas concentrations (Braconnot et al., 2007; Renssen et al., 2009). The lower methane concentration during MH corresponds to a decreased radiative forcing of 0.07 W m^{-2} during the MH (Otto-Bliesner et al., 2006). The maximum increase in June insolation at 65° N for the MH is 40 W m^{-2} (Berger, 1978). For comparison the increase in radiative forcing due to a doubling of the present day atmospheric CO_2 concentration is 3.7 W m^{-2} (Solomon et al., 2007).

2.2 Models

The mid-Holocene (MH) and pre-industrial (PI) control simulations from 11 models part of the PMIP2 ensemble have been analysed in this study. Only models for which sea ice and temperature data were available in the PMIP2 database were included. The PMIP2 experiments were performed with the same model versions as used for future climate simulations performed for the Climate Modelling Intercomparison Project 3 (CMIP3), but in most cases the PMIP2 simulations were run at lower resolution (Braconnot et al., 2007). Only two modelling centres have submitted simulations run with the same model version for both the CMIP and PMIP experiments. For these two models the MH simulations are also compared to a future scenario of 1 % increase per year of the atmospheric CO_2 concentration to doubling. The 11 models are listed in Table 3 with the acronym used in this paper, their model name as used in the PMIP2 database, modelling centre and the atmospheric and oceanic resolution. The models are all coupled atmosphere-ocean global circulation models, but with different resolutions. The sea ice models are of different complexity. Three of the models, FGOALS, FOAM, and UBRIS include only thermodynamic sea ice models, the other 8 models have thermodynamic and dynamic sea ice models.

The variables analysed in this work is the sea ice concentration, sea ice thickness, 2 m temperature and surface temperature. Near surface wind or wind stress was not available in the database and the variables are therefore not included in the further analysis. The spin-up method varies between the different modelling centres. However, for each experiment the simulation should be run long enough for any trends to be small. For information about the model drifts, see Braconnot et al. (2007).

The analysis is performed on the 100 last model years submitted to the database, except for CCSM and GISS, for which only 50 yr of data were submitted. To facilitate model inter-comparison the model output was interpolated to a common regular ($0.5° \times 1°$) latitude–longitude grid using bilinear interpolation.

3 Thermodynamic considerations

We will here use a simple thermodynamic model to qualitatively examine the response of the Arctic sea ice cover to the changes in insolation between the pre-industrial era and the mid-Holocene. The analysis is based on the toy model of Thorndike (1992).

3.1 Four-step model

Ignoring sea-ice dynamics, Thorndike (1992) argued that the seasonal thermodynamic changes of the sea ice can conceptually be described as a four step cycle; comprised by a cooling, growing, warming, and melting period, respectively. To illustrate we use the seasonal cycle for CCSM, see Fig. 1. The three annual cycles shown in the figure is the seasonal cycle in the (a) PI, (b) MH and (c) $2 \times CO_2$ climates. The blue line is the cold season; here the surface temperature is sufficiently low so that ice can grow at the base of the ice floe. At this stage, the ice gains thickness. For the yellow line, the temperature above the ice starts to increase. In this part of the cycle the ice is warming up. During this warming period the ice neither looses nor gains any more thickness. The warming continues until the temperature directly over the ice reaches the melting point, the red part of the curve. The melting takes place at the top of the ice. The length of red line corresponds to the melt season of the ice. For the cyan line the temperature drops below 0 °C. The ice starts to cool down, and continues so until the surface temperature has dropped sufficiently for the ice thickness to increase again at the bottom of the ice.

In an idealised scenario these four steps give a rectangle. If the mean state of the ice is thick, the rectangle will be more elongated, with small changes in the thickness during the growth and melt seasons, compare to cycle (a) in Fig. 1. If the mean thickness of the ice decreases, the seasonal variation in sea ice thickness will increase, and the cycle will be more like a square in the shape, compare to cycle (b) and (c) in Fig. 1. This is due to the isolation effects of the ice. In reality the rectangle is not a perfect rectangle, some cooling will still occur in the winter season when the ice is growing

thicker, and the ice will gain some thickness during the warming period, and vice versa when we have melting and warming, and the rectangle will be somewhat skewed due to isolation effects in the ice (Thorndike, 1992).

3.2 Two–step model

As demonstrated by Thorndike (1992), an illuminating simplification of the four-step cycle is to divide the year into only two seasons: One melt season, when the temperature above the ice is at the melting point, and one growing season, when the temperature is below the melting point. This two-step sea ice model of Thorndike will now be used to examine the response of sea ice to changes in the orbital forcing. In the model, which is described in detail by Thorndike (1992) and Bitz and Roe (2003) the ice melting M and growth G, in meters, are given by

$$M = \frac{\tau_M}{L}\left(-F_{LW} + F_W + (1 - \alpha)\overline{F}_{SW}\right),$$ (1)

$$G(h) = \frac{\tau_G}{L}(-F_{LW} + F_W),$$ (2)

where τ_M/τ_G is the length of the melt/growth season, F_{LW} the net upward flux of long-wave radiation, F_W the oceanic heat flux at the base of the ice, h is the annual-mean ice thickness, α the albedo, and

$$\overline{F}_{SW} = \frac{1}{\tau_M}\int_{t_o}^{t_o+\tau_M} F_{SW}(t')dt',$$ (3)

the mean insolation over the melt season, which range from t_0 to $t_0 + \tau_M$[1]. The net upward longwave radiation from the ice is based on a linearization of the Stefan-Boltzmann law, accounting for a seasonally dependent optical depth and down welling

---

[1]Following Bitz and Roe (2003) an atmospheric albedo of 0.44 is used to relate the top of the atmosphere insolation to the surface insolation F_{SW}.

Full Screen / Esc

Printer-friendly Version

Interactive Discussion

radiation due to atmospheric heat transport convergence, denoted D. In the melt season, when the surface temperature is at the freezing point (i.e. $T = 0\,^\circ$C), the net longwave radiation is given by

$$F_{LW}^M = A/n_M - D/2, \tag{4}$$

and in the growth season by

$$F_{LW}^G = [A + BT(h)]/n_G - D/2. \tag{5}$$

Here, n_M and n_G are the optical depths for the melt and the growth season, respectively, and the surface ice temperature in the growth season is given by

$$T(h) = \left(\frac{n_G h}{n_G k + Bh}\right)\left(-\frac{A}{n_G} + \frac{D}{2}\right). \tag{6}$$

The ice thickness dependence of the surface ice temperature stems from the assumption of a steady heat conduction through the ice during the growth season. An important consequence of Eq. (6) is that the temperature and hence the ice growth decreases with increasing ice thickness. Thus, thin ice grows faster than thick ice, which proves to be central for the model's response to changes of the forcing. For simplicity, the albedo of the ice is taken to be constant, an approximation that is reasonable for thick ice, but fails when the ice becomes thinner. The standard model parameters are given in Table 2.

The insolation change between the MH to the PI era can affect the sea ice in two ways: (i) via changes in the integrated absorbed solar radiation $\overline{F}_{SW}$; and (ii) via changes of the length of the melt season τ_M. The precessional cycle chiefly involves a redistribution of the insolation over the year. When the northern summer occurs at perihelion, the peak insolation is higher but Kepler's second law dictates that the summer season is shorter (e.g. Pierrehumbert, 2010; Hartman, 1994). As a result, the integrated summer insolation hardly changes with the precession alone, i.e. $\tau_M \overline{F}_{SW}$ is

essentially invariant. It should be noted, however, that a shorter melt season leads to enhanced melting in this model. The reason is energy loss of the ice due to the thermal radiation: a shorter melt season implies a reduced net emission of thermal radiation, leaving more energy for melting. Clearly, a short melt season, during which the surface ice temperature is at the melting point, reduces the annual mean ice surface temperature and hence the longwave energy loss driving the ice growth. Using Eq. (1), the effect of a shortening of the melt season under preserved integrated insolation can be calculated as $\delta M = \delta\tau_M(-F_{LW}^M + F_W)/L$. For the present choice of parameters, a one-month reduction of the melt season yields an increase in the melting of about 0.4 m. As we will discuss below, however, the changes in the melt season length between PI and MH are small enough to be neglected.

The higher axis tilt in the MH also affected the seasonal distribution of the insolation, illustrated in Fig. 2. To qualitatively consider how the combined effect of the precession and tilt affects the melt season, we assume that melting occurs when the top of the atmosphere daily insolation exceeds some threshold value. Figure 2a illustrates, for MH and PI, the length of the melt season as a function of threshold insolation at 65° N. Notably, the difference in melt season length between the two periods is only about a few days, except for near the maximum insolation threshold. We have repeated the calculations for higher latitudes as well and found that the difference in melt season length between the two periods gets even smaller as the north pole is approached. This suggests that regardless of the insolation threshold for the onset of melting, the changes in the length of the melt season should be negligible for the difference in melting between MH and PI. Thus, we will follow Thorndike (1992) and Bitz and Roe (2003) and take the melt and the growth seasons to each be six moths long when analysing the sea-ice response to the orbitally induced insolation changes.

Figure 2b shows the ice melt as a function of the insolation threshold. The ice melt attains a maximum for a melt season length of about five months. This is a result of the effect of the melt-season length on the total longwave radiation loss described above. The important result, however, is that the changes in ice melt between MH and PI is

Full Screen / Esc

Printer-friendly Version

Interactive Discussion

fairly insensitive to the assumed threshold insolation. As shown in Fig. 2b, the sea ice melting is about 0.2 m higher in MH than in PI, a value which is essentially constant from 65° N and polewards.

To estimate the response of the sea-ice thickness to an increased melting of 0.2 m, we follow Bitz and Roe (2003) and consider perturbations on the steady state conditions, specified by $M = G(h)$. This yields $\delta h \frac{\partial G}{\partial h} = \delta M$. From this relation, the change in annual-mean sea ice thickness (δh) for a given change in melting (δM) as a function of the annual mean sea ice thickness (h) is straightforward to compute in the Thorndike model (see Bitz and Roe, 2003, for details). Figure 3 shows the change in annual-mean sea ice thickness for an increase of the melting of 0.2 m as a function of the equilibrium thickness. For comparison, the effect of an annually constant downward energy flux increase of 4 W m^{-2}, representing roughly a CO_2 doubling, is shown. This effect translates to an increased melting of about 0.4 m. Figure 3 shows that the change in sea ice thickness is larger for thicker equilibrium thicknesses. As shown by Bitz and Roe (2003), however, the effect of a CO_2 doubling is in this model reduced by a negative feedback due to the adjustment of the ice surface temperature: The ice surface warms which enhances the upward longwave radiation, partly compensating for the reduction in ice growth due to the CO_2 induced increase in downward longwave radiation. In the Thorndike model, this leads to a cooling of the atmospheric column, which strongly reduces the increase in downward longwave radiation. If this local negative feedback is included, the effect of CO_2 doubling yields an increased of melting of about 0.2, i.e. comparable to the insolation changes between the MH and the PI.

In summary, we expect that if local thermodynamics control the sea-ice response, Fig. 3 will essentially describe the response of the sea-ice thickness in the between the MH and PI in the PMIP2 simulations. However, additional feedbacks included in the models can cause a stronger as well as weaker response of the sea ice in the simulations. In particular, the neglected albedo dependence of the sea ice thickness could result in a transition to a regime without summer sea ice in the mid Holocene (e.g., Abbot et al., 2011; Moon and Wettlaufer, 2012).

4 Arctic sea ice in the PMIP2 simulations

4.1 Pre-industrial climate

In the model mean the sea ice thickness cover is thickest at the north pole, with a maximum sea ice thickness of 4 m. The ice covers the entire Arctic basin and extends south into the Greenland and Barents Sea. The 11 models show a large model-model variability in the pre-industrial sea ice conditions. The simulated sea ice area for March and September is listed in Table 4. The sea ice area is here defined as the area of all grid cells with a sea ice concentration greater than 15 %. Also included in the table is the mean sea ice area for the period 1979–2007, determined from the satellite observations (Cavalieri et al., 2008). The model mean March sea ice cover is slightly more extensive in PI compared to observations for the period 1979–2007. For the September sea ice, the difference in the model mean and observed sea cover is larger. The sea ice coverage in the FGOALS model immediately stands out from the other models, not only is the simulated sea ice cover too extensive, but also the seasonal variation in the sea ice cover is also very low. The September sea ice cover in the FGOALS model extends as far south as Great Britain in the PI climate. The FGOALS model is also known to simulate a too extensive sea ice cover for present day (Zhang and Walsh, 2006). Excluding FGOALS from the model mean gives PI sea ice areas for both March and September closer to present day observations.

The simulated sea ice thickness for the 11 models and the model mean is shown in Fig. 4. In September, the maximum sea ice thickness in the Arctic region varies from 1.5 m in CSIRO1.0 to more than 5 m in CCSM and FGOALS. Also the thickness distribution among the models varies a lot. Some models (CCSM, GISS, MRIfa, MRInfa) have the thickest ice in the region north of Greenland, in accordance with present observations. ECBILT has the thickest ice in the Chukchi Sea and East Siberian Sea, the two CSIRO models, FOAM, MIROC and UBRIS have the thickest ice close to the north pole. For comparison, the observed sea ice cover from 1979–2007 is included in Fig. 5.

The figure shows the sea ice margin, which can be compared to the extent shown in Fig. 4.

In the PI climate the models have the lowest September temperatures over Greenland (not shown), due to the presence of the Greenland ice sheet and its high elevation,

5   else the lowest temperatures are simulated over ocean in regions of thick sea ice, along the northern coast of Greenland and otherwise over the north pole. On the Atlantic side of the Arctic, the isotherms follow the sea ice edge, and the 15 % sea ice limit is located between the −3 and 0 °C isotherm.

4.1.1   Seasonal cycle

10   The amplitude of the seasonal cycle in sea ice area is model dependent, see Fig. 6a. The model-model spread is largest in the annual maximum sea ice area (February–April) and smallest in the annual minimum sea ice area (August–October). In general, models with relatively small annual average sea ice area as compared to the other models exhibit smaller amplitude annual cycles in sea ice area. The majority of the

15   models have the largest sea ice area in March (one model has larger area in February, one in April), the minimum ice area occurs in September or October.

Along the sea ice margin the ice is thinnest and the sea ice concentration is lowest, the largest amplitude seasonal cycle in both sea ice extent and thickness occurs here. The ice albedo feedback causes the relatively thin ice in the ice margins to melt off

20   during summer. In winter a larger amount of heat can be conducted from the ocean to the atmosphere, and this favours the ice growth. The blue curves in Fig. 7 show the seasonal variation of the sea ice thickness and temperature directly above the ice north of 80° N in the PI climate. All models have perennial ice in this region. Models with thicker annual average sea ice in this region generally have a smaller amplitude

25   annual cycle in sea ice thickness than do models with thinner annual average sea ice. During the summer, the models with thinner ice looses more ice, in order to maintain an equilibrium thickness, the ice will therefore grow more during winter. The thicker ice

will have to change less in order to maintain its equilibrium thickness, and show smaller variations in the thickness.

4.2 Sensitivity to solar forcing

The sea ice area is reduced for all models in September, see Table 4. In the analysis of the response to MH forcing conditions only statistically significant differences at the 95 % confidence level are considered. The statistical significance is determined using a Student's t-test. The reduction in sea ice area is strongest during the winter months (January–April), see Fig. 6b. In addition to the reduction in sea ice area, the simulated sea ice thickness is also reduced in the MH climate. The strongest reduction occurs in summer as displayed in Fig. 8, and the maximum reduction in sea ice thickness in the model mean is about 1 to 1.5 m. The largest reduction in the sea ice thickness occurs in the region where the ice was thickest in the control simulation. The exception to this is FOAM, this model has the thickest ice closest to the north pole, but have modest reduction in thickness in this region.

In winter, the majority of the models get a thinning of the ice cover: The thinning is however smaller than for the summer ice (not shown). The exceptions are the two CSIRO models, which do not experience any thinning in the winter ice cover, and UBRIS, which gets thicker ice in the MH winter simulation.

In the model mean the MH September climate becomes warmer in entire region north of 60° N, with a maximum warming of 3 °C in the central Arctic Ocean. The strongest warming occurs in the Barents Sea region, Northeast Greenland, and the Canadian Archipelago, see Fig. 9. FOAM is the model with the most homogenous warming north of 60° N. The two MRI models have the strongest warming, these models mainly warm in the Barents, Kara, Laptev, and East Siberian Sea. In March, some models show a general cooling north of 60° N (not shown), however, a few models have regions with substantial warming (more than 4 °C). A few models also get a winter warming in the Barents Sea region and/or Canadian Archipelago, but the warming is not as consistent among the models as the summer warming (not shown). The

response in the average sea ice thickness north of 80° N is also seen in Fig. 7. The annual average sea ice thickness is decreased and the amplitude of the annual cycle is increased in all models. Further, the annual average sea ice thickness response is larger in the models with thickest ice in the PI climate.

5 Discussion

5.1 Sensitivity to solar forcing

The largest difference in sea ice thickness between MH and PI climate occurs where the ice was initially thickest, which can be seen by comparing Figs. 4 and 8. This relationship is displayed in Fig. 10 where the annual average thickness change is shown as a function of the annual average equilibrium ice thickness in the simple two–step model and for the region north of 80° N in the PMIP2 simulations. The simulations with a doubling of CO_2 are also included in Fig. 10. In agreement with the two-step model result, the annual average thickness change is larger in these simulations than in the MH simulations. The seasonal variation in sea ice thickness and surface temperature increases even more in the simulations forced with a doubling of CO_2, and also under these conditions the model with the thickest ice has the strongest response to the changes in the greenhouse gas concentration. This result is in agreement with the inference from the simple two-step model described in Sect. 3.2 (see also Fig. 3).

5.2 Comparison to proxy data

Proxy data indicate a smaller sea ice cover in the early to mid-Holocene. This study only considers the mid-Holocene, and for this period the reduction in ice thickness and extent off the north-eastern coast of Greenland is modest in all models, in disagreement with the findings of Funder et al. (2011) and Jakobsson et al. (2010). There could be several explanations for this. First, the sea ice is highly variable and the beach ridges

may have been produced during one single year of ice-free conditions. This type of year-to-year variability is not found in this region in any of the models though, possibly indicative of too small variability in the simulated Arctic sea ice. The lack of variability in the models is also discussed in Lohmann et al. (2012). Second, the bias in the

5 PI sea ice extent and thickness distribution may also influence the models ability to simulate the MH sea ice extent. Even if the models were to have the correct sensitivity to the MH forcing, a too extensive sea ice cover in the control climate may bias the simulated MH sea ice cover. Third, the timing of the period with less ice in this region according to the two studies is sometime between 8.5 and 6 ka BP, whereas the mid-

10 Holocene simulation only represents the latter part of this interval, and this could cause a mismatch between proxy data and models.

If the region northeast of Greenland had less ice during the early to mid-Holocene, this was probably not the mean state of the ice, but extreme events. This is further supported by the fact that some proxies suggest less ice (Funder et al., 2011; Jakobsson

15 et al., 2010) and some suggest more ice (de Vernal et al., 2008) during the same time periods.

6 Conclusions

The objective of this study was to assess the Arctic sea ice in the mid-Holocene climate simulated by the models in the PMIP2 database. The result from 11 models is included

20 in this work. The main findings are

– The control climates simulated by the 11 models are rather different. Exposed to the same forcing the sea ice cover, thickness distribution and spatial temperature pattern between the models diverge. The sea ice areal extent in the PI simulations ranges from 10.1 to 28.2 (7.01 to 24.6) million km^{-2} in March (September), and

25   the maximum sea ice thickness range from 1.5 to more than 5 (1 to more than 5) m in March (September).

- The models agree on the main differences between the MH and PI climate. In all models the total ice cover is smaller and thinner in mid-Holocene in both March and September. The response in the sea ice area is stronger in late winter (February–April) whereas the response in sea ice thickness is stronger in late summer (August–October).

- All models experience an increase in 2 m temperature north of 60° N in September, compared to the control climate. In March the majority of the models experience a slight cooling in the Arctic, some models however, get regions with strong warming also in March.

- The region north of 80° N is covered with perennial sea ice both in the PI and MH simulations. In this region the amplitude of the seasonal cycle in the ice thickness is larger in the mid-Holocene climate. The mean ice thickness is also less in the warmer climate. In an even warmer climate, here represented as a doubling of the atmospheric CO_2, the ice gets even thinner, and the seasonal amplitude increases more. This is in accordance to what is expected from the simple thermodynamic model of Thorndike. The model says that the response in the model should be stronger under the forcing caused by a doubling of the atmospheric CO_2 compared to the forcing during MH.

- The seasonal variation of the sea ice thickness, and the model response to the perturbation in the forcing from PI to MH the sea ice is mainly govern by thermodynamics. The fact that all models respond in a similar way even though their ice models are of different complexity supports this.

- Proxy data indicates that the sea ice cover in the Arctic could have been substantial smaller during the early and mid-Holocene. None of the models get a reduced sea ice cover northeast of Greenland in the MH simulation.

References

Abbot, D. S., Sibler, M., and Pierrehumbert, R. T.: Bifurcatios leading to summer Arctic sea ice gloss, J. Geophys. Res. 116, D19120, doi:10.1029/2011JD015653, 2011. 3456

Berger, A. L.: Long-term variations of daily insolation and Quaternary climatic changes, J. Atmos. Sci., 35, 2362–2367, 1978. 3450

Bitz, C. M. and Roe, G. H.: A mechanism for the high rate of sea ice thinning in the Arctic Ocean, J. Climate, 17, 3623–3632, 2003. 3449, 3453, 3455, 3456

Braconnot, P., Otto-Bliesner, B., Harrison, S., Joussaume, S., Peterchmitt, J.-Y., Abe-Ouchi, A., Crucifix, M., Driesschaert, E., Fichefet, Th., Hewitt, C. D., Kageyama, M., Kitoh, A., Laîné, A., Loutre, M.-F., Marti, O., Merkel, U., Ramstein, G., Valdes, P., Weber, S. L., Yu, Y., and Zhao, Y.: Results of PMIP2 coupled simulations of the Mid-Holocene and Last Glacial Maximum – Part 1: experiments and large-scale features, Clim. Past, 3, 261–277, doi:10.5194/cp-3-261-2007, 2007. 3448, 3450, 3451

Cavalieri, D., Parkinson, C., Gloersen, P., and Zwally, H. J.: Sea ice concentration from Nimbus-7 SMMR and DMSP SSM/I-SSMIS Passive Microwave Data, [1979–2008], Boulder, Colorado USA: National Snow and Ice Data Centre, Digital Media, 2008. 3447, 3457, 3475

de Vernal, A., Hillaire-Marcel, C., Solinac, S., and Radi, T.: Reconstructing sea ice conditions in the Arctic and Sub-Arctic prior to human observations, in: Arctic Sea Ice Decline: Observations, Projections, Mechanisms, and Implications, edited by: Weaver, E., AGU Monograph Series, 180, 27–45, 2008. 3448, 3449, 3461

Funder, S., Goosse, H., Jepsen, H., Kaas, E., Kjær, K. H., Korsgaard, N. J., Larsen, N. K., Linderson, H., Lysaa, A., Möller, P., Olsen, J., and Willerslev, E.,: A 10 000-year record of

Title Page

Abstract | Introduction

Conclusions | References

Tables | Figures

◄ | ►

◄ | ►

Back | Close

Full Screen / Esc

Printer-friendly Version

Interactive Discussion

Arctic Ocean sea-ice variability – View from the beach, Science, 333, 747–750, 2011. 3449, 3460, 3461

Gordon, C., Cooper, C., Senior, C. A., Banks, H., Gregory, J. M., Johns, T. C., Mitchell, J. F. B., and Wood, R. A.: The simulation of SST, sea ice extents and ocean heat transports in a version of the Hadley Centre coupled model without flux adjustments, Clim. Dynam., 16, 147–168, 2000. 3469

Hartman, D. L.: Global Physical Climatology, Academic Press, California, 1994. 3454

Holland, M. M., Serreze, M. C., and Stroeve, J.: The sea ice mass budget of the Arctic and its future change as simulated by coupled climate models, Clim. Dynam., 34, 185–200, doi:10.1007/s00382-008-0493-4, 2008. 3448

Jacob, R., Schafer, C., Foster, I., Tobis, M., and Andersen, J.: Computational design and performance of the Fast Ocean Atmosphere Model: Version 1, in: The 2001 International Conference of Computational Science, 175–184, 2001. 3469

Jakobsson, M., Long, A., Ingólfsson, Ó., Kjær, K. H., and Spielhagen, R. F.: New insights on Arctic Quaternary climate variability from paleo-records and numerical modelling, Quaternary Sci. Rev., 29, 3349–3358, 2010. 3449, 3460, 3461

K-1-Model-Developers: K-1 Coupled GCM (Miroc description), Tech. rep., CCSR/NIES/FRCGC, 2004. 3469

Kwok, R. and Rothrock, D. A.: Decline in Arctic sea ice thickness from submarine and ICESat records: 1958–2008, Geophys. Res. Lett., 36, L15501, doi:10.1029/2009GL039035, 2009. 3447

Levitus, S., Boyer, T. P., Conkright, M. E., O'Brien, T., Antonov, J., Stephens, C., Stathoplos, L., Johnson, D., and Gelfeld, R.: NOAA Atlas NESDIS 18, World Ocean Database 1998, Vol. 1, Introduction, 1998. 3450

Lohmann, G., Pfeiffer, M., Laepple, T., Leduc, G., and Kim, J.-H.: A model-data comparison of the Holocene global sea surface temperature evolution, Clim. Past Discuss., 8, 1005–1056, doi:10.5194/cpd-8-1005-2012, 2012. 3461

Moon, W. and Wettlaufer, J. S.: On the existence of stable seasonally varying Arctic sea ice in simple models, J. Geophys. Res., 117, C07007, doi:10.1029/2012JC008006, 2012. 3456

Notz, D. and Marotzke J.: Observations reveal external driver for Arctic sea-ice retreat, Geophys. Res. Lett., 39, L08502, doi:10.1029/2012GL051094, 2012. 3447

Otto-Bliesner, B. L., Brady, E. C., Clauzet, G., Tomas, R., Levis, S., and Kothavala, Z.: Last Glacial Maximum and Holocene climate in CCSM3, J. Climate, 19, 2526–2544, 2006. 3450, 3469

Petoukhov, V. and Semenov, V. A.: A link between reduced Barents-Kara sea ice and cold winter extremes over northern continents, J. Geophys. Res., 115, D21111, doi:10.1029/2009JD013568, 2010. 3448

Phipps, S. J.: The CSIRO Mk3L Climate system model, Tech. rep., Antarctic Climate and Ecosystems CRC, University of Tasmania, Institute of Antarctic and Southern Ocean Studies, 2006. 3469

Pierrehumbert, R. T.: Principles of Planetary Climate, Cambridge Univ. Press, NY, 2012. 3454

Polyak, L., Alley, R. B., Andrews, J. T., Bringham-Grette, J., Cronin, T. M., Darby, D. A., Dyke, A. S., Fritzpatrick, J. J., Funder, S., Holland, M., Jennings, A. E., Miller, G. H., O'Regan, M., Savelle, J., Serreze, M., St.John, K., White, J. W. C., and Wolff, E.: History of sea ice in the Arctic, Quaternary Sci. Rev., 29, 1757–1778, 2010. 3448, 3449

Renssen, H., Goosse, H., Fichefet, T., Brovkin, V., Driesschaert, E., and Wolk, F.: Simulating the Holocene climate evolution at northern high latitudes using a coupled atmosphere-sea ice-ocean-vegetation model, Clim. Dynam., 24, 23–43, 2005. 3469

Renssen, H., Seppä, H., Hein, O., Roche, D. M., Goosse, H., and Fichefet, T.: The spatial and temporal complexity of the Holocene thermal maximum, Nat. Geosci., 2, 411–414, doi:10.1038/NGEO513, 2009. 3450

Rothrock, D. A., Zhang, J., and Yu, Y.: The Arctic sea ice thickness anomaly of the 1990s: A consistent view from observations and models, J. Geophys. Res., 1008, 3083, doi:10.1029/2001JC001208, 2003. 3447

Serreze, M. C., Holland, M. M., and Stroeve, J.: Perspectives on the Arctic's shrinking sea ice cover, Science, 3115, 1533–1536, 2007. 3447

Schmidt, G. A., Ruedy, R., Hansen, J. E., Aleinov, I., Bell, N., Bauer, M., Bauer, S., Cairns, B., Canuto, V., Cheng, Y., Del Genio, A., Faluvegi, G., Friend, A. D., Hall, T. M., Hu, Y., Kelley, M., Kiang, N. Y., Koch, D., Lacis, A. A., Lerner, J., Lo, K. K., Miller, R. L., Nazaewnko, L., Oinas, V., Perlwitz, J., Perlwitz, J., Rind, D., Romanou, A., Russell, G. L., Sato, M., Shindell, D. T., Stone, P. H., Sun, S., Tausnev, N., Thresher, D., and Yao, M.-S.: Present-day atmospheric simulations using GISS ModelE: Comparison to in situ, satellite and reanalysis data, J. Climate, 19, 153–192, 2006. 3469

Title Page

Abstract | Introduction

Conclusions | References

Tables | Figures

|◀ | ▶|

◀ | ▶

Back | Close

Full Screen / Esc

Printer-friendly Version

Interactive Discussion

Solomon, S., Qin, D., Manning, M., Chen, Z., Marquis, M., Averyt, K. B., Tignor, M., and Miller, H. L. (Eds.): Climate Change 2007, The Physical Science Basis, Contribution of Working Group 1 to the Fourth Assessment Report of the Intergovernmental Panel on Climate Change, 2007. 3447, 3450

5 Stroeve, J., Holland, M. M., Meier, W., Scambos, T., and Serreze, M.: Arctic sea ice decline: Faster than forecast, Geophys. Res. Lett., 34, L09501, doi:10.1029/2007GL029703, 2007. 3447, 3448

Thorndike, A. S.: A toy model linking atmospheric thermal radiation and sea ice growth, J. Geophys. Res., 97, 9401–9410, 1992. 3449, 3452, 3453, 3455, 3456, 3462

10 Yu, Y. Q., Zhang, X. H., and Guo, Y. F.: Global coupled ocean-atmosphere general circulation models in Lasg/Iap, Adv. Atmos. Sci., 21, 444–455, 2004. 3469

Yukimoto, S., Noda, A., Kito, A., Hosaka, M., Yoshimura, H., Uchiyama, T., Shibata, K., Arakawa, O., and Kusunoki, S.: Present-day climate and climate sensitivity in the Meteorological Research Institute Coupled Gcm Version 2.3 (MRI-CGCM2.3), J. Meteorol. Soc. Jpn., 84, 333–

15 363, 2006. 3469

Zhang, Q., Sundqvist, H. S., Moberg, A., Körnich, H., Nilsson, J., and Holmgren, K.: Climate change between the mid and late Holocene in northern high latitudes – Part 2: Model-data comparisons, Clim. Past, 6, 609–626, doi:10.5194/cp-6-609-2010, 2010. 3449

Zhang, X. and Walsh, J. E.: Toward a seasonally ice-covered Arctic Ocean: Scenarios from the
20 IPCC AR4 model simulations, J. Climate, 19, 1730–1757, 2006. 3448, 3457

Full Screen / Esc

Printer-friendly Version

Interactive Discussion

Table 1. Solar and greenhouse gas forcing for pre-industrial control and mid-Holocene, following the PMIP2 protocol.

	PI	MH
Eccentricity	0.016724	0.018682
Obliquity	23.446°	24.105°
Angular precession	102.04°	0.87°
CO_2	280 ppm	280 ppm
CH_4	760 ppb	650 ppb
N_2O	270 ppb	270 ppb
CFC	0	0
O_3	Modern, 10 DU	Modern, 10 DU

Table 2. Parameters used in simple model.

A	σT^4 with $T = 273$ K	320 W m^{-2}
B	$4\sigma T^3$ with $T = 273$ K	4.6 W m^{-2}
D	atmospheric heat transport	100 W m^{-2}
F_{SW}	summer mean shortwave insolation at 65° N	W m^{-2}
F_{W}	ocean heat flux	2 W m^{-2}
h	annual mean ice thickness	variable
k	thermal conductivity	2 W m^{-1} K^{-2}
L	latent heat of fusion	3×10^8 J m^{-3}
n_M/n_G	optical depth summer/winter	2.5 or 3.25
α	sea ice albedo	0.65
$\tau_{M/G}$	length of melt/growth season	182.5 days

Table 3. The 11 model simulations used in this study and the modelling centres. Also atmospheric and oceanic resolutions are listed. The difference between MRIfa and MRInfa is that the latter does not have any flux adjustment.

Model	Modelling centre	Model reference	Resolution atmosphere long × lat (levels)	Ocean long × lat (levels)
CCSM	National Centre for Atmospheric Research (NCAR), USA	Otto-Bliesner et al. (2006)	T42 (26)	1° × 1° (40)
CSIRO1.0	Commonwealth Scientific and Industrial Research Organisation, Australia	Phipps (2006)	R21 (18)	5.6° × 3.2° (21)
CSIRO1.1	Commonwealth Scientific and Industrial Research Organisation, Australia	Phipps (2006)	R21 (18)	2.8° × 3.2° (21)
ECBILT	Koninklijk Nederlands Meteorologisch Instituut, Netherlands	Renssen et al. (2005)	T21 (3)	3° × 3° (21)
FGOALS	LASG, Institute of Atmospheric Physics, China	Yu et al. (2004)	T42 (26)	1° × 1° (33)
FOAM	Centre for Climatic Research, USA	Jacob et al. (2001)	R15 (18)	2.8° × 1.4° (16)
GISS	NASA Goddard Institute for Space Studies, USA	Schmidt et al. (2006)	4° × 5°(17)	4° × 5° (17)
MIROC	Centre for Climate System Research, Japan	K-1-Model-Developers (2004)	T42 (20)	1.4° × 0.5° (43)
MRIfa	Meteorological Research Institute Japan	Yukimoto et al. (2006)	T42 (30)	2.5° × 0.5° (23)
MRInfa	Meteorological Research Institute Japan	Yukimoto et al. (2006)	T42 (30)	2.5° × 0.5° (23)
UBRIS	Hadley centre, UK	Gordon et al. (2000)	3.74° × 2.5° (19)	1.25° × 1.25° (19)

Table 4. Total sea ice covered area in March and September, PI and MH. A grid cell is considered covered with sea ice if the sea ice concentration is larger than 15 %. The models with statistically significant reductions in sea ice area between MH and PI are marked boldface. The model mean excluding (including) FGOALS. Observations for the period 1979–2007 are included for comparison.

Model	Sea ice area 10^6 km^2 March PI	MH-PI	Sea ice area 10^6 km^2 September PI	MH-PI
CCSM	19.2	−6.78	9.09	**−0.851**
CSIRO-1.0	11.0	**−1.57**	8.08	**−0.705**
CSIRO-1.1	10.1	**−0.722**	7.71	**−0.509**
ECBILT	11.7	−1.03	9.16	**−0.501**
FGOALS	28.2	−10.6	24.6	**−6.97**
FOAM	23.7	**−10.5**	10.7	**−0.236**
GISS	21.5	−2.84	14.7	**−0.990**
MIROC	14.7	−1.20	8.36	**−0.551**
MRIfa	15.2	**−3.29**	8.50	**−1.76**
MRInfa	27.2	**−11.8**	10.6	**−1.47**
UBRIS	21.7	−5.39	7.01	**−1.24**
Model mean	17.6 (18.6)	−4.59 (−5.17)	9.39 (10.8)	−0.88 (−1.46)
Observations 1979–2007	17.3			7.86

Title Page

Abstract | Introduction

Conclusions | References

Tables | Figures

|◄ | ►|

◄ | ►

Back | Close

Full Screen / Esc

Printer-friendly Version

Interactive Discussion
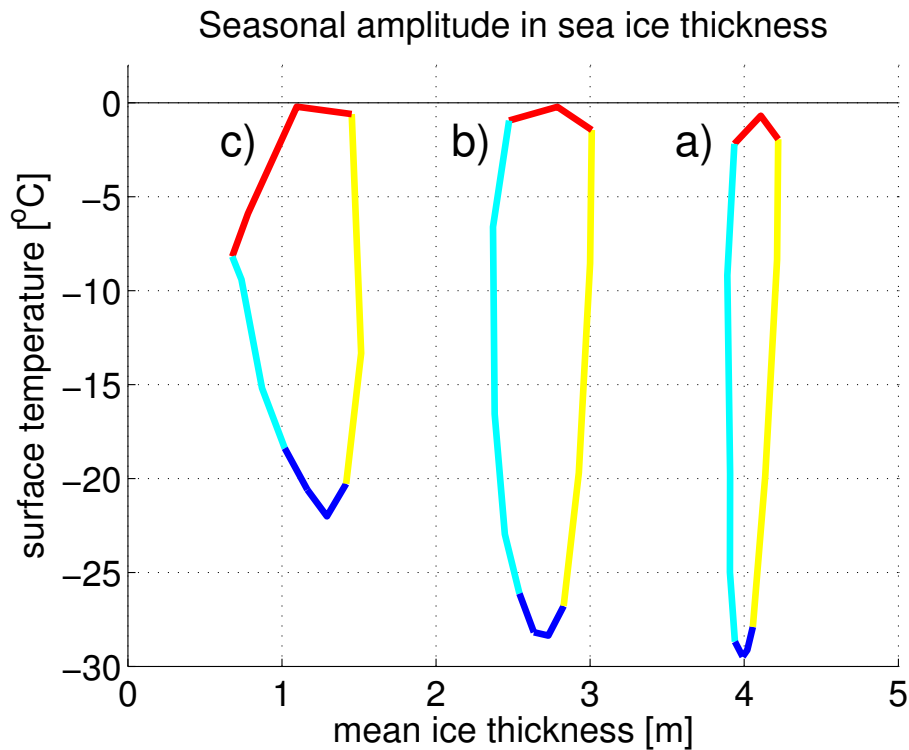
Fig. 1. Seasonal variation of sea ice thickness and surface temperature in the region north of 80° N for the CCSM model. The blue line represents the growing season, yellow is warming, red is melting and cyan is the cooling season. The three curves are (a) PI, (b) MH, and (c) 2 × CO_2 climate. Note that seasonal progression of the sea ice is anti-clockwise in the thickness-temperature diagram.

Title Page

Abstract | Introduction

Conclusions | References

Tables | Figures

|◄ | ►|

◄ | ►

Back | Close

Full Screen / Esc

Printer-friendly Version

Interactive Discussion
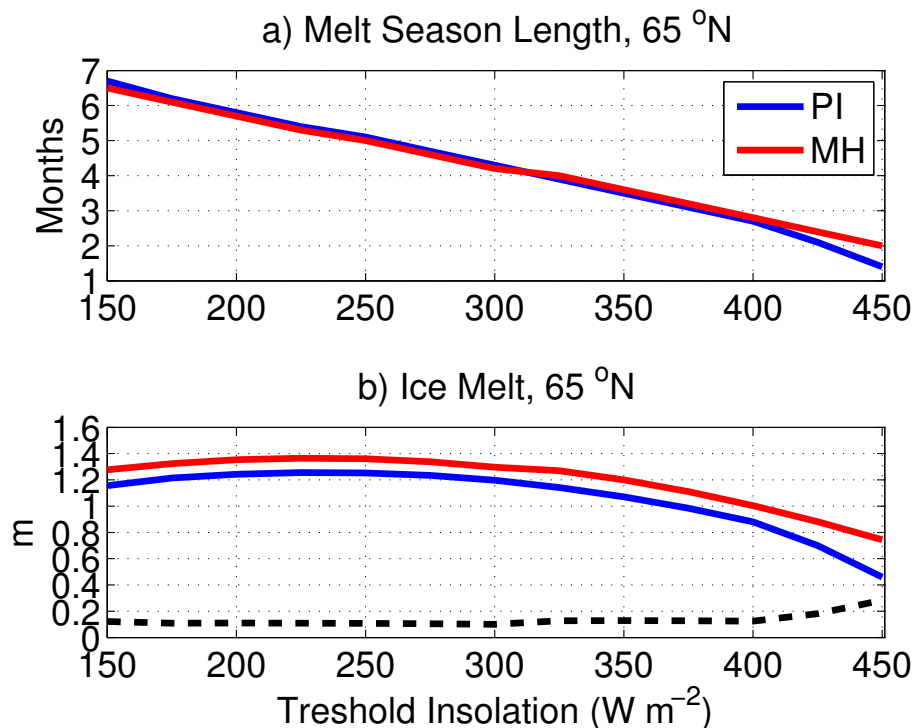
Fig. 2. Melt season length **(a)** and sea ice melt **(b)** as a function of a threshold of the insolation at the top of the atmosphere at 65° N. The melt season length is defined as the time (in months) when the insolation is above the threshold specified on the x-axis. The corresponding sea ice melt (in meters) is calculated from Eq. (1); see the text for details. The blue and the red lines refer to the PI and MH respectively; and the black dashed line in **(b)** show the difference in sea ice melt between MH and PI.
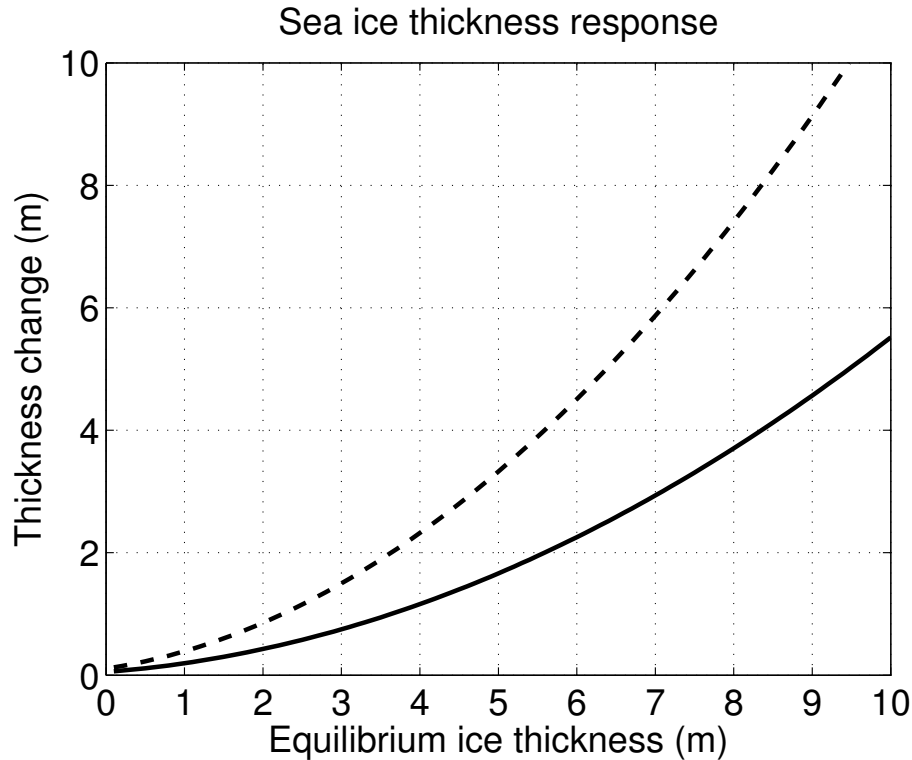
Fig. 3. The change in sea ice thickness as a function of the equilibrium sea ice thickness computed from Thorndike's model; see text for details. The solid line shows the model response for the change in insolation between PI and MH, corresponding to an increase of the sea ice melting of about 0.2 m. The dashed line represents the response of $2 \times CO_2$ forcing, corresponding to an increase of the sea ice melting of about 0.4 m.

Printer-friendly Version

Interactive Discussion
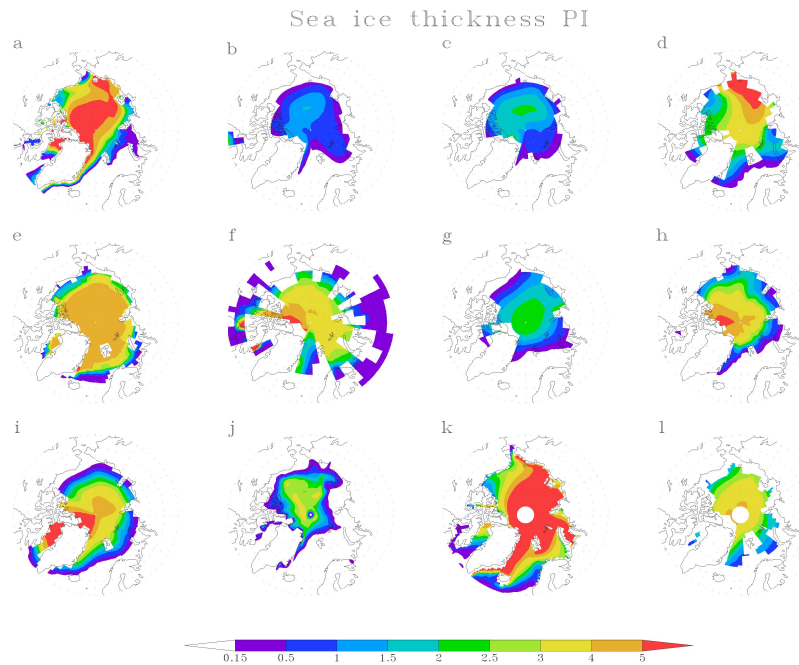
Fig. 4. Sea ice thickness in the pre-industrial control climate. Models are **(a)** CCSM, **(b)** CSIRO-1.0, **(c)** CSIRO-1.1 **(d)** ECBILT, **(e)** FOAM, **(f)** GISS, **(g)** MIROC, **(h)** MRIfa, **(i)** MRInfa, **(j)** UBRIS, **(k)** FGOALS and **(l)** model mean. Only grid cells with sea ice thicker than 15 cm is plotted.
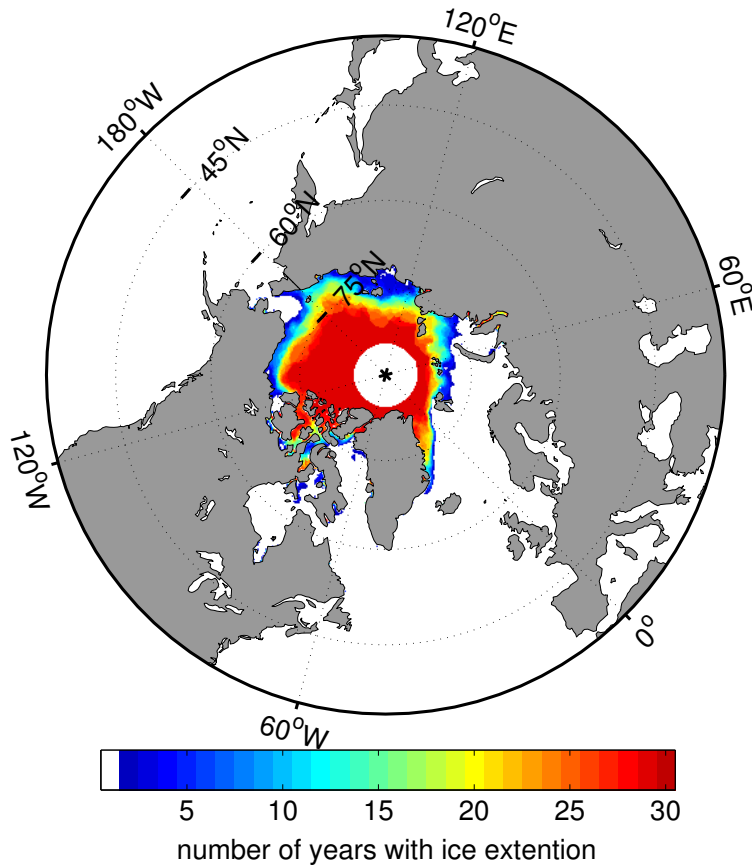
Fig. 5. Observed September Arctic sea ice cover from 1979–2007. The colour scale indicates the number of years with sea ice cover. The data is from Cavalieri et al. (2008).

Title Page

Abstract | Introduction

Conclusions | References

Tables | Figures

|◄ | ►|

◄ | ►

Back | Close

Full Screen / Esc

Printer-friendly Version

Interactive Discussion
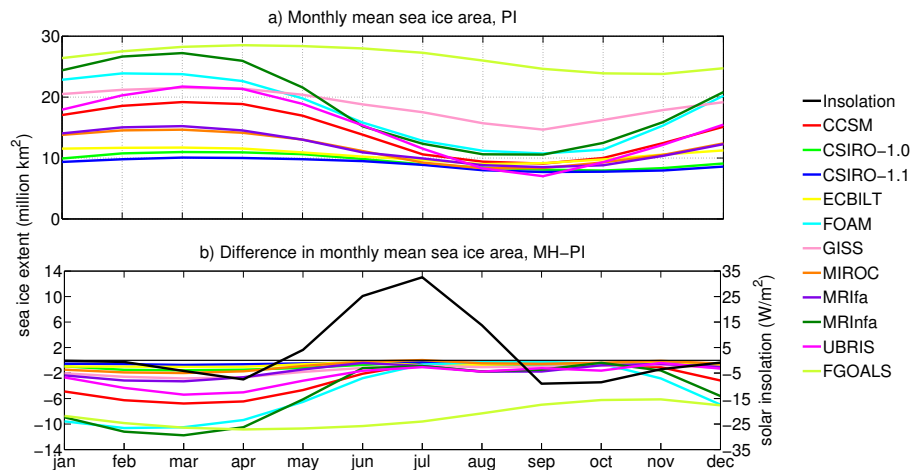
Fig. 6. (a) Monthly mean sea ice area for PI simulations. **(b)** Difference in monthly mean sea ice area from MH to PI. Also included is the difference in solar insolation at 65° N.
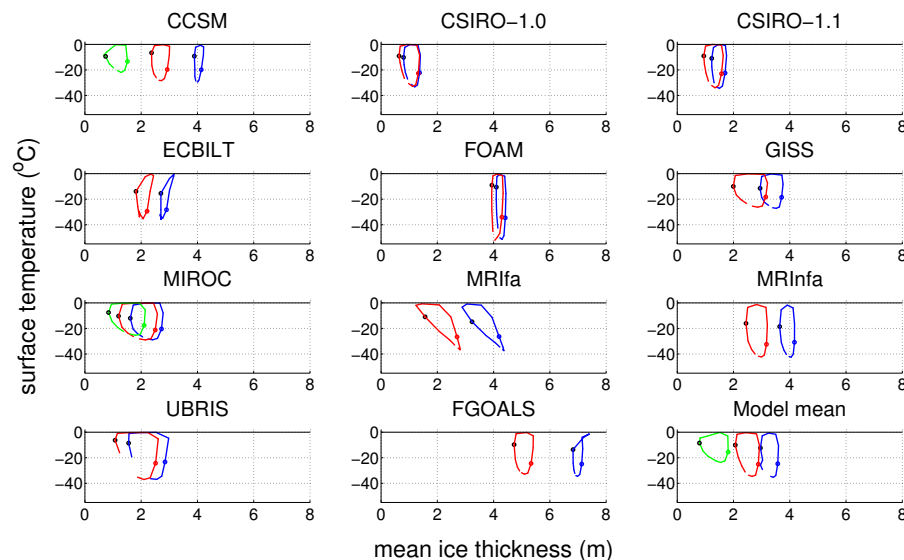
Fig. 7. Seasonal variation in sea ice thickness and surface temperature for the region north of 80° N. The months March and September are marked with a coloured and black dot, respectively. The blue line is for the control climate and the red line for the mid-Holocene climate. The green line represents a 2 × CO_2 climate.
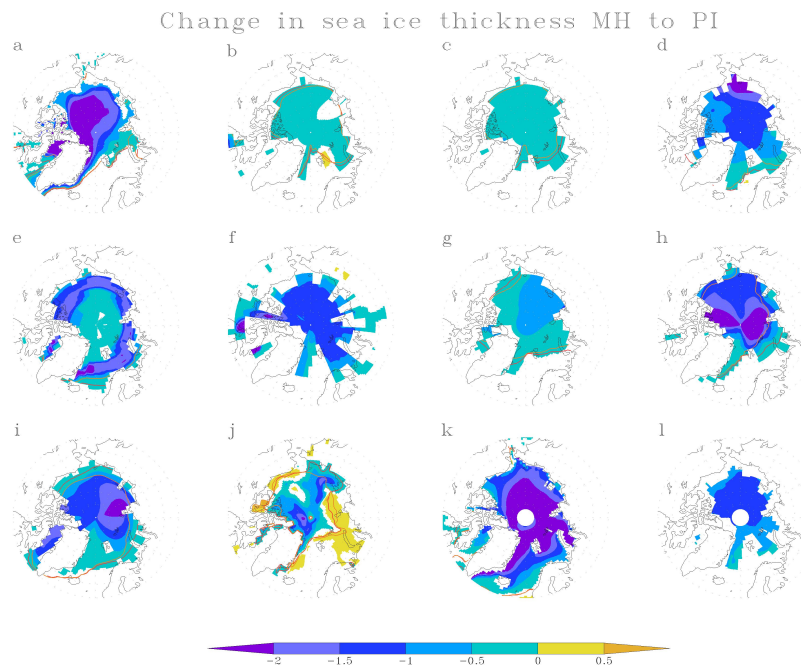
Fig. 8. Difference in sea ice thickness between mid-Holocene and pre-industrial climate. Models are same as in Fig. 4. Only statistically significant changes are plotted. The red line is the sea ice edge (sea ice thickness thicker than 15 cm) in the PI climate and the orange line is the sea ice edge in the MH climate.

Back | Close

Full Screen / Esc
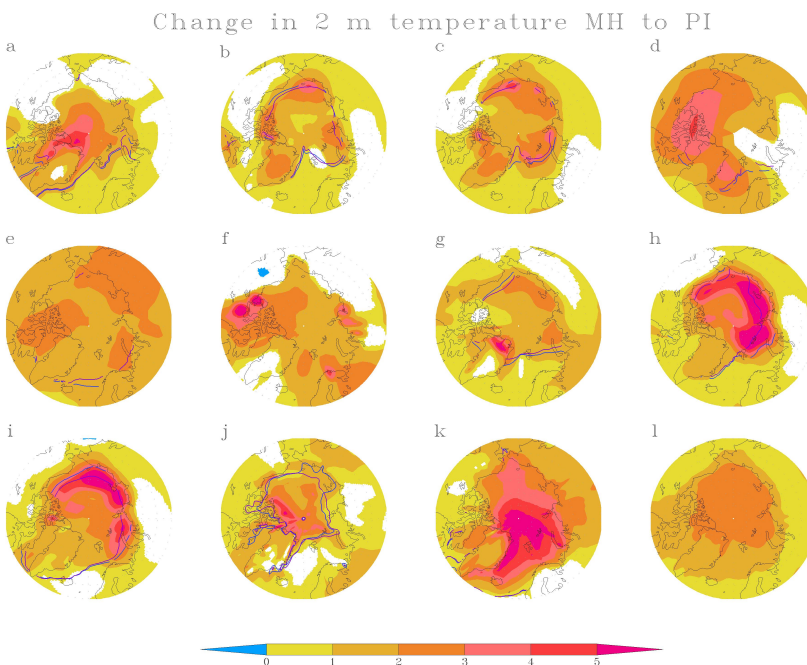
Printer-friendly Version

Interactive Discussion

Fig. 9. Difference in 2 m temperature between MH and PI climate. Models are same as in Fig. 4. Only statistically significant changes are plotted. The blue line is the sea ice edge (sea ice thickness thicker than 15 cm) in the PI climate and the purple line is the sea ice edge in the MH climate.
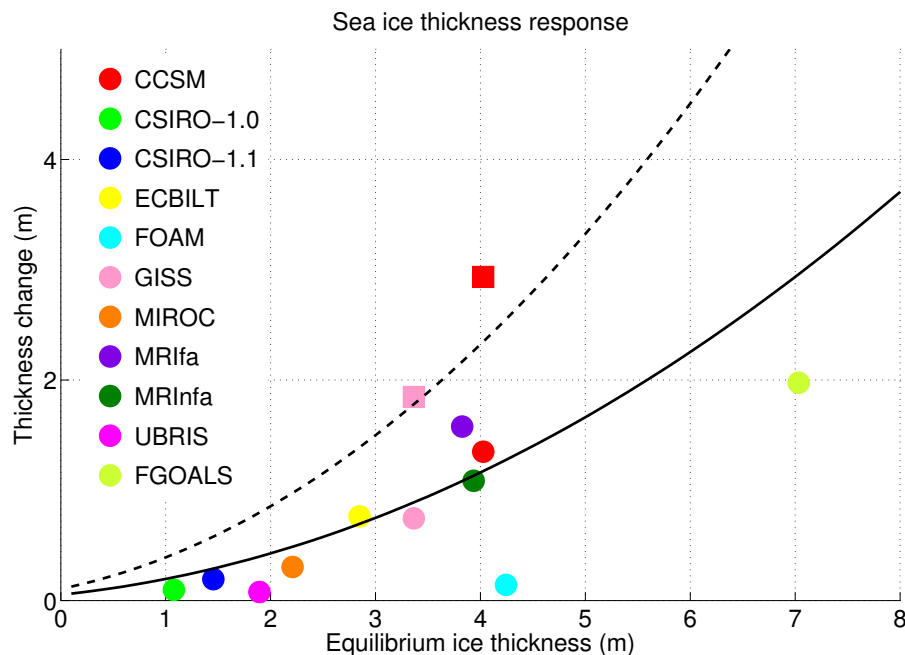
Fig. 10. Difference in equilibrium sea ice thickness north of 80° N and the change in equilibrium thickness from mid-Holocene to pre-Industrial (circles), and for $2 \times CO_2$ to pre-industrial (squares). The grey lines are the thickness change as determined from the simple model, for the MH forcing (solid) and $2 \times CO_2$ (dashed line).

Title Page

Abstract | Introduction

Conclusions | References

Tables | Figures

|◀ | ▶|

◀ | ▶

Back | Close

Full Screen / Esc

Printer-friendly Version

Interactive Discussion